Ultra-Wideband (UWB) Frequency-Reconfigurable Phased Array

Gengming Wei [(1)], Yi He [(1)], Richard W. Ziolkowski [(2)], and Y. Jay Guo [(1)]
(1) University of Technology Sydney, Sydney, Australia, wud9032@163.com
(2) University of Arizona, Tucson, USA, ziolkows@arizona.edu

***Abstract*—This paper introduces an innovative ultra-wideband (UWB) frequency-reconfigurable tightly-coupled dipole array (FR-TCDA). It achieves high radiation efficiency and a wide beam-scanning range through a unique reconfigurable layer and a customized wide-angle impedance matching (WAIM) structure. The reconfigurable layer effectively converts out-of-phase ground-plane reflections into in-phase ones with minimal insertion loss, allowing seamless operation across two contiguous frequency bands. A prototype confirmed its two reconfigurable states yield two overlapping sub-bands that span 0.37-0.93 GHz and 0.85-5.85 GHz, respectively, and jointly provide an overall combined 15.8:1 bandwidth covering 0.37-5.85 GHz with VSWR < 3 and a radiation efficiency higher than 95%. The WAIM structure is designed with dual-level double-sided capacitively loaded loops (DLDS-CLLs), enabling enhanced scanning performance with scan angles up to ±70° in the E-/D-planes and ±50° in the H-plane. Its properties make this phased array well-suited for UWB applications requiring high radiation efficiency and broad scan volumes.**

I. Introduction

The increasing demand for high data capacity has spurred considerable interest in antenna arrays capable of supporting broader RF spectra. To address this need, the deployment of collocated multi-band antenna arrays has become a widely adopted strategy. However, this type of antenna array often suffers from substantial cross-band interference due to the close proximity of its antennas working in different bands on the same platform [1]. Despite advancements in various filtering and frequency-selective techniques aimed at this issue, effectively management of cross-band interference across ultra-wideband (UWB) coverage remains a significant challenge [2], [3], [4].

In contrast, UWB antenna arrays provide a more efficient solution by delivering continuous spectrum coverage through a single, integrated deployment that eliminates the need for cross-band interference suppression. Tightly-coupled dipole arrays (TCDAs) have gained wide attraction in this regard with advantages that include UWB spectrum coverage, compact sizes with low profiles, and wide scan volumes [5]. This type of array typically achieves relative bandwidths of up to 5:1 through the coupling between neighboring dipole arms [5], [6], and can be pushed to approximately 10:1 by enhanced coupling [7]. However, further expanding the bandwidth beyond 10:1 presents significant challenges. The primary obstacle are the short-circuit resonance effects caused by the existence of the ground plane (GP) [5], [8]. Integrating highly lossy materials such as resistive layers can address the short-circuit issue and extend the bandwidth up to 46:1; however, they reduce the radiation efficiency significantly [9], [10].

In this work, we present an innovative frequency-reconfigurable TCDA (FR-TCDA) that addresses the conflict between further bandwidth extension and array efficiency. By incorporating a reconfigurable layer, the developed array operates a combined 15.8:1 bandwidth that includes two contiguous sub-bands — 0.37−0.93 GHz and 0.85−5.85 GHz — while maintaining a high radiation efficiency of 95%. Additionally, a specialized wide-angle impedance matching (WAIM) structure based on dual-level, double-sided capacitively loaded loops (DLDS-CLLs) enables an enhanced scanning performance, with scan angles up to ±70° in the E-/D-planes and ±50° in the H-plane with VSWR < 3. A 14×14 array prototype was fabricated and measured; the measurement results confirmed the simulated ones.

II. Array Design

Fig. 1(a) shows the configuration of the array's unit cell and indicates key components including the DLDS-CLLs WAIM structure, reconfigurable layer, and balun and shorting pins. Fig. 1(b) displays a corresponding finite array example with 3×3 elements.

A. Frequency Reconfiguration with High Radiation

The array achieves frequency reconfiguration across a broad overall operating bandwidth with high radiation

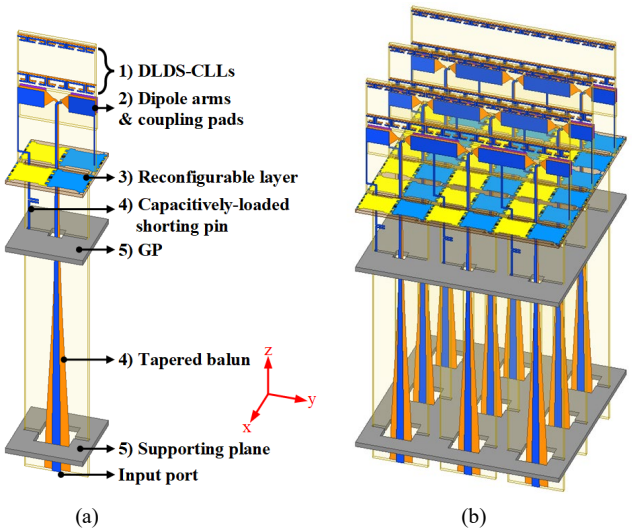

Fig. 1. Isometric view of the developed FR-TCDA. (a) Unit cell. (b) A 3×3 finite array.

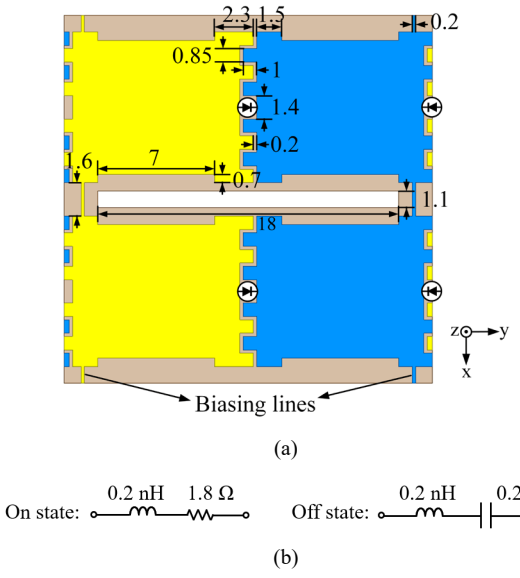

Fig. 2. Unit cell of the reconfigurable layer (a) Top view. (b) Equivalent circuits for both states of the selected PIN diode.

efficiency through a unique reconfigurable layer. This reconfigurable layer realizes phase manipulation of the reflected waves, converting out-of-phase reflections into desired in-phase ones with low insertion loss. By switching the states of the diodes, the reconfigurable layer functions across two contiguous frequency bands.

Fig. 2(a) shows the unit cell of the reconfigurable layer. It consists of patches with interdigital edges, with PIN diodes set between adjacent patches. The yellow and blue patches on the reconfigurable layer are connected to DC+ and DC- signals to facilitate the diodes' control. The diodes used are Infineon BAR90-02ELS [11]; its equivalent circuits for both states are shown in Fig. 2(b).

We analyzed the reflection responses of the reconfigurable layer through a simplified unit cell model. Fig. 3(a) shows its structure, and Figs. 3(b) and 3(c) illustrate its reflection magnitude and phase responses for both the on and off states. The results indicate that switching the diodes from the off-state to the on-state shifts the in-phase reflection band from lower to higher frequencies, with minimal reflection magnitude losses—below 0.015 dB in the off-state and 0.35 dB in the on-state. These losses are significantly lower than those observed with typical resistive sheets that exhibit a reflection loss of 3.8 dB [9]. Consequently, this enables frequency reconfiguration of the array while maintaining high radiation efficiency. As shown in Fig. 4, the whole array achieves two contiguous operating bands with VSWR < 3. Their frequencies span 0.37−0.93 GHz in the off-state and 0.85−5.85 GHz in the on-state. A high radiation efficiency that exceeds 95% for both states is attained. For the sake of clarity, the off-state and on-state are hereinafter referred to as the lower-band state (LS) and higher-band state (HS), respectively.

B. Enhanced Scanning Performance

Through the incorporation of DLDS-CLLs, the array realizes reduced impedance variations when its beam is scanned at various angles in different planes. To demonstrate this effect, we compare the input impedance results of the

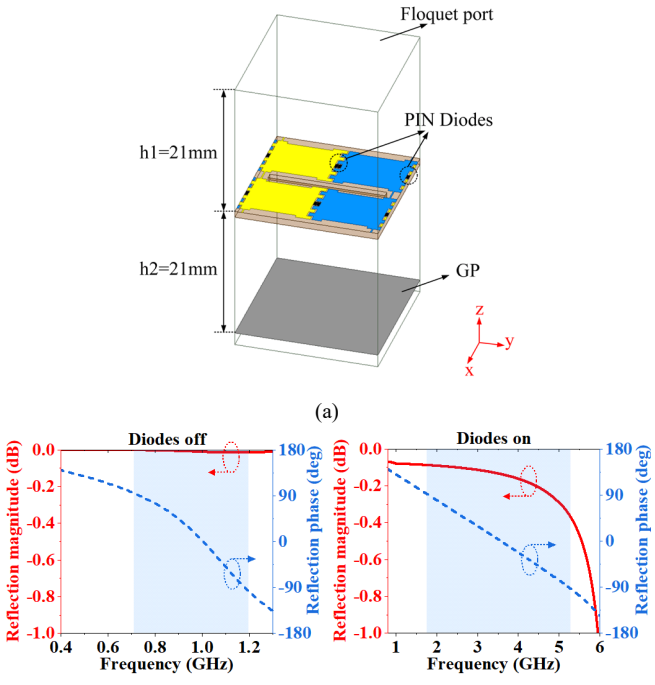

Fig. 3. Simulated results. (a) Unit cell of the simplified model. Reflection wave response of this simplified model when the diodes are in (b) off-state and (c) on-state.

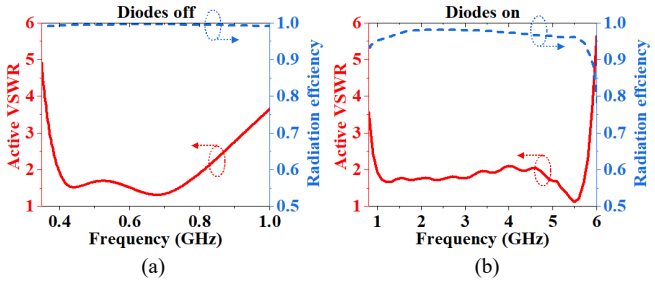

Fig. 4. Radiation efficiency and active VSWR of the developed array in the broadside direction when the diodes are in the (a) off-state and (b) on-state.

dipole array without and with the DLDS-CLLs, as illustrated in Fig. 5. All Smith charts have been normalized to 150 Ω. Figs. 5(a) and 5(b) show the impedance results of the two states when the beam is scanned up to ± 45° in the E-/H-planes. As demonstrated, the impedance loci of the dipole array with DLDS-CLLs when scanning in both the E- and H-planes are more confined than those of the array without DLDS-CLLs, indicating improved matching performance.

C. UWB Feeding Without Unwanted Resonances

The array is fed by Klopfenstein tapered baluns combined with capacitance-loaded shorting pins, providing stable UWB performance without unwanted resonances throughout the entire operating bandwidth. The tapered balun, with a total length of 115 mm, transforms the 50 Ω unbalanced input into a 150 Ω balanced output. The capacitance inserted on the shorting pin is specifically designed to suppress unwanted resonances across the operating bandwidth of both states.

Fig. 6(a) illustrates the progression of the shorting pin. After incorporating the balun, a common-mode resonance was

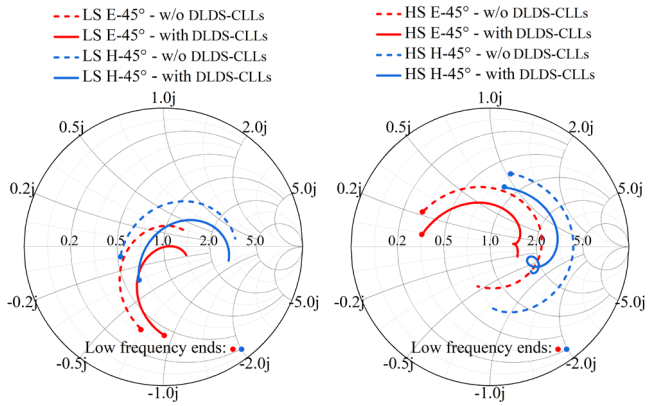

(a) (b)

Fig. 5. Comparison of input impedance results of the developed array without and with the DLDS-CLLs. (a) E-/H-45° scanning case in the LS. (b) E-/H-45° scanning case in the HS.

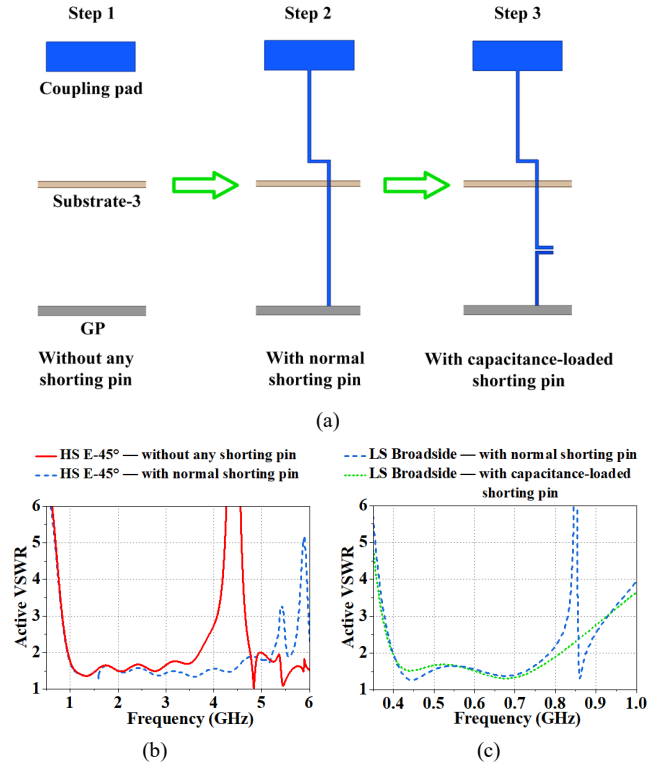

Fig. 6. Shorting pin evolution. (a) Design progression. (b) Active VSWRs of the array unit cell for the HS E-45° scanning case with shorting pin designs in step 1 and step 2. (c) Active VSWRs of the array unit cell for the LS broadside case with shorting pin designs in step 2 and step 3.

observed around 4.3 GHz for the HS E-45° scanning case. To address this issue, normal shorting pins were first introduced, as depicted in step 2 in Fig. 6(a). A comparison of the array VSWRs in Fig. 6(b) verifies the effective elimination of the 4.3 GHz resonance in the HS after integrating the normal shorting pin. However, this adjustment led to a new resonance at 0.84 GHz for the LS broadside case. A capacitance was then added to the shorting pin to address this, as shown in step 3 of Fig. 6(a). From the array VSWRs of steps 2 and 3 in Fig. 6(c), this measure successfully suppressed the resonance at 0.84 GHz.

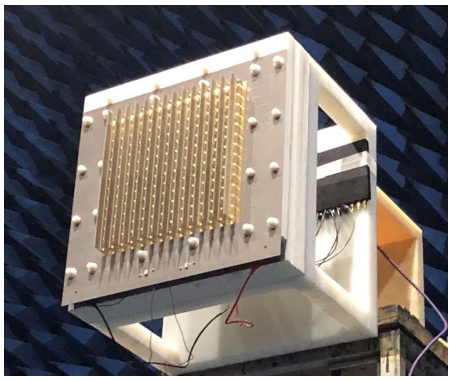

Fig. 7. The fabricated array prototype with 14×14 elements.

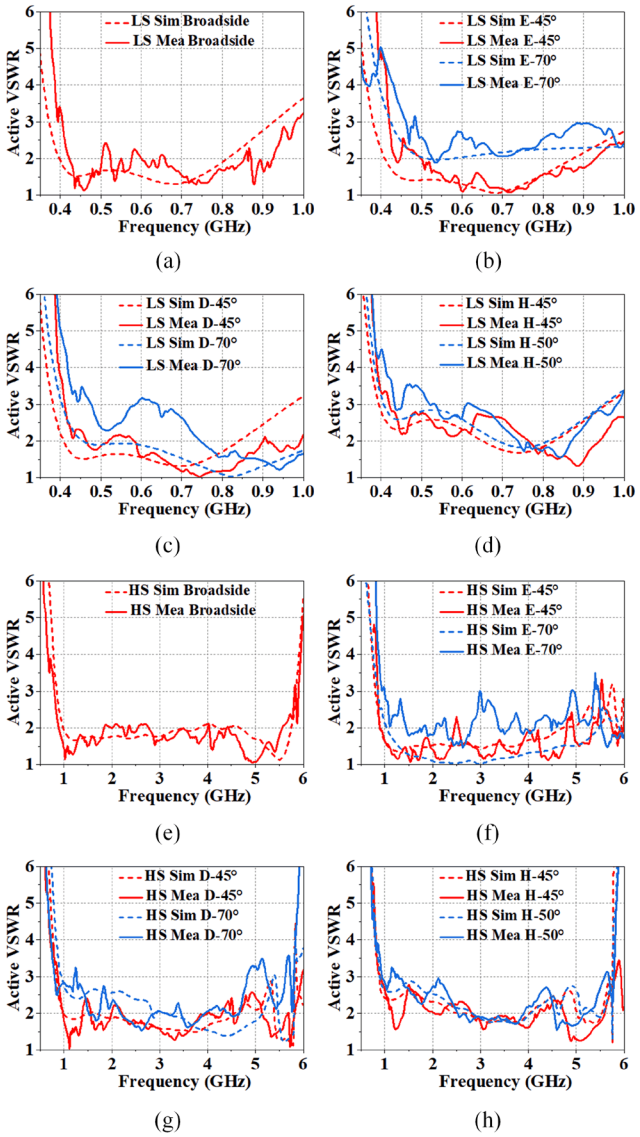

Fig. 8. Simulated and measured active VSWRs for broadside and various scanning cases in the E-/D-/H-planes in the (a)–(d) LS, and (e)-(h) HS.

Consequently, it was confirmed that the final feeding design successfully tuned out all unwanted resonances outside the operating bandwidth.

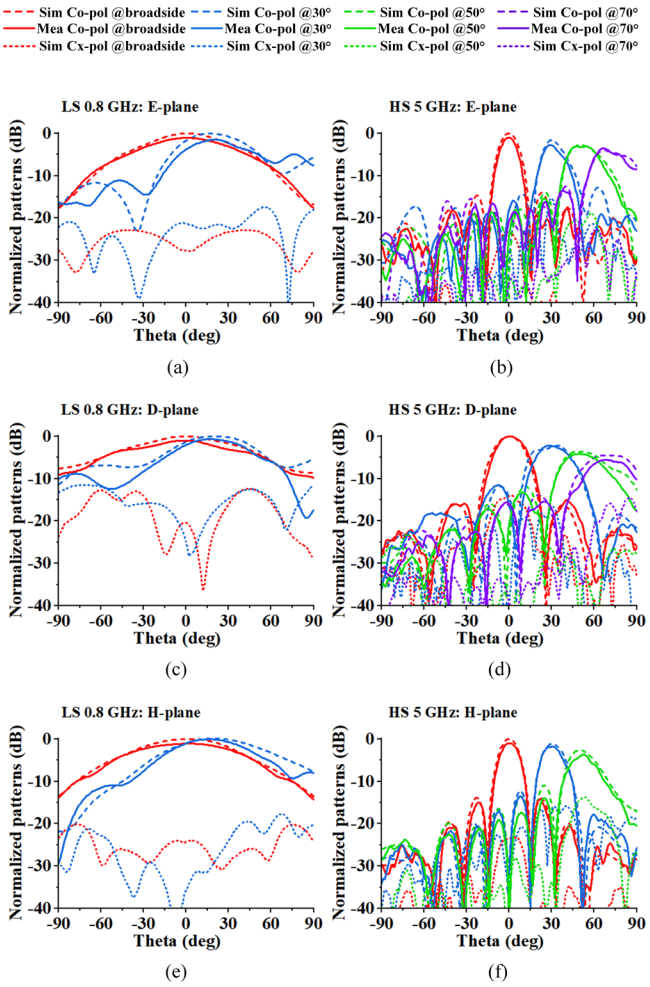

Fig. 9. Simulated and measured patterns of the fabricated array prototype for broadside and various scanning cases in the E-/D-/H-planes at (a), (c), (e) 0.8 GHz in the LS, and (b), (d), (f) 5.0 GHz in the HS.

III. Discussion

Fig. 7 shows a picture of the fabricated array prototype, which consisted of 14×14 elements. Fig. 8 compares the simulated and measured active VSWRs of the center element located at the 7th row and 7th column. At broadside, the two states of the developed array cover with a VSWR < 3 an overall 15.8:1 bandwidth, spanning from 0.37 to 5.85 GHz (two contiguous bandwidths: 0.37-0.93 GHz in the LS and 0.85-5.85 GHz in the HS). The scanning performance of the array with its VSWR < 3 covers a 13.7:1 bandwidth from 0.42 to 5.77 GHz (two contiguous bandwidths: 0.42-0.93 GHz in the LS and 0.90-5.77 GHz in the HS) when scanning up to ±70° in the E-/D-planes and ±50° in the H-plane. Fig. 9 shows radiation patterns at two example frequencies of 0.8 GHz and 5 GHz. A comparison of the measured and simulated results confirms good radiation performance achieved in both states.

IV. Conclusion

This paper presented a frequency-reconfigurable tightly-coupled dipole array (FR-TCDA) that achieved an overall 15.8:1 bandwidth with two reconfigurable states. Its innovative reconfigurable layer facilitated seamless switching between its two contiguous low and high frequency sub-bands; it elegantly addressed the challenge of the GP-induced short-circuit effect without the high cost of sacrificing efficiency associated with resistive layer solutions. Its DLDS-CLLs WAIM structure provided enhanced impedance matching performance during wide-angle scanning while maintaining lightweight characteristics. The measured 14×14 array prototype demonstrated high radiation efficiency and wide-angle beam scanning performance in very good agreement with its simulated performance characteristics. The developed FR-TCDA offers significant improvements over conventional UWB phased arrays and is well-suited for UWB applications requiring high radiation efficiency and broad scan volumes.

References

[1] Y. J. Guo and R. W. Ziolkowski, *Advanced Antenna Array Engineering for 6G and Beyond Wireless Communications*, 1st ed. Wiley, 2021.

[2] R. Chao Dai, S. Sun, H. Su, and X. Y. Zhang, "Analysis and design of dual-modal filtenna for dismountable aperture-shared array," *IEEE Trans. Antennas Propagat.*, vol. 72, no. 6, pp. 4806–4817, Jun. 2024.

[3] S.-Y. Sun, C. Ding, W. Jiang, and Y. J. Guo, "Simultaneous suppression of cross-band scattering and coupling between closely spaced dual-band dual-polarized antennas," *IEEE Trans. Antennas Propagat.*, vol. 71, no. 8, pp. 6423–6434, Aug. 2023.

[4] Y. He, C. Ding, C. Chang, G. Wei, and Y. J. Guo, "A bowl-shaped filtering antenna with wideband cross-band scattering mitigation for dual-band base stations," *IEEE Trans. Antennas Propag.*, 72, no. 8, pp. 6723–6728, Aug. 2024.

[5] B. A. Munk, "Broadband Wire Arrays," in *Finite Antenna Arrays and FSS*, Hoboken, NJ, USA: John Wiley & Sons, Inc., 2005, pp. 181–213.

[6] J. P. Doane, K. Sertel, and J. L. Volakis, "Bandwidth limits for lossless planar arrays over ground plane," *Electron. Lett.*, vol. 48, no. 10, p. 540, 2012.

[7] I. Tzanidis, K. Sertel, and J. L. Volakis, "Interwoven spiral array (ISPA) with a 10: 1 bandwidth on a ground plane," *IEEE Antennas and Wireless Propag. Lett.*, vol. 10, pp. 115–118, 2010.

[8] C. A. Balanis, *Modern antenna handbook*. John Wiley & Sons, 2011.

[9] W. F. Moulder, K. Sertel, and J. L. Volakis, "Superstrate-enhanced ultrawideband tightly coupled array with resistive FSS," *IEEE Trans. Antennas Propag.*, vol. 60, no. 9, pp. 4166–4172, Sep. 2012.

[10] A. D. Johnson, J. Zhong, S. B. Venkatakrishnan, E. A. Alwan, and J. L. Volakis, "Phased array with low-angle scanning and 46:1 bandwidth," *IEEE Trans. Antennas Propag.*, vol. 68, no. 12, pp. 7833–7841, Dec. 2020.

[11] Infineon Technologies. BAR90-02ELS. [Online]. Available: https://www.infineon.com/cms/en/product/rf/rf-diode/rf-pin-diode/antenna-switch/bar90-02els/